RSC Advances

PAPER

View Article Online
View Journal | View Issue

Cite this: *RSC Adv.*, 2023, **13**, 16663

Deep red emission from rare-earth-free calcium aluminozincate phosphor with the substitution of Cr^{3+} ion

Sumandeep Kaur, Videsh Kumar and A. S. Rao *

Chromium-doped calcium aluminozincate phosphor with a distinct amount of chromium was prepared *via* the sol–gel technique. The phase analysis and morphological study along with optical properties were conducted on the prepared material. The room temperature luminescent traits of the sample were studied in detail under 540 nm excitation wavelength. The deep red emission was confirmed from the CIE coordinates calculated using emission data. The decay curves were recorded to calculate the lifetime values for the aforementioned powder samples. The temperature-dependent luminescent characteristics were also investigated to identify the activation energy and thermal stability. The quantum yield was also calculated using luminescence spectra and found to be relatively good for the present phosphor. All of the investigated studies specified above signify that the synthesized phosphor is well suited as a red emitter in lighting and display devices.

Received 31st March 2023
Accepted 14th May 2023

DOI: 10.1039/d3ra02129g

rsc.li/rsc-advances

1. Introduction

Inorganic materials incorporated with transition metal or rare earth ions, also known as phosphors, exhibit luminescence. These luminescent materials find applications in various fields, *e.g.*, sensors, solar cells, plant growth, display, lighting, biophotonic applications, and anti-counterfeiting.[1–7] Usually, rare earth ions such as Eu^{3+}, Tb^{3+}, Sm^{3+}, and Dy^{3+} ions are widely used in lighting applications. However, there are some limitations of using these rare earths as dopants in luminescent materials. These rare earths are quite expensive and require some harsh conditions such as high temperature and high pressure[8] to synthesize phosphors. Also, these rare earths have high photon re-absorption in the visible region owing to various transition levels available in rare earth ion doped phosphors and decline the output of the phosphors. Moreover, they have narrow and weak absorption bands due to parity-forbidden transitions, which reduce the absorption efficiency.[9] All of these drawbacks provide an opportunity for the development of rare-earth-free phosphors for different applications.

The alternative approach of designing a color emitter in the hue of the visible electromagnetic spectrum is to use transition metal ions, such as Bi^{3+}, Cr^{3+}, Mn^{4+}, and Mn^{2+} as dopants in the inorganic material as these ions possess blue, red, and green emissions, respectively.[9–14] There are many reports on the Cr^{3+} and Mn^{4+}-doped luminescent materials developed for wLEDs as a red component, which is required to improve the color rendering index of wLEDs.[8] The transition metals have a tendency to give variable color emission based on different hosts, as the transitions that take place in the transition metal ion-doped phosphors are influenced by the crystal field environment, including the type of ligand coordination, variation in functional groups, and covalency.[15,16] The energy levels in the transition metal ions are described by the Tanabe–Sugano diagram. The vacant d-orbital of Cr^{3+} ($3d^3$) provides the arrangement of energy levels based on the crystal field and site occupation in such a way that it can give red and near infrared emission.[12,17,18] Qiang M. *et al.* reported on ceramic phosphor $ZnAl_2O_4$ doped with Cr^{3+} ions and studied the luminescence properties, as far red luminescence is important for plant growth.[19] Liu *et al.* reported on chromium ion-doped magnesium tantalate having emission in the NIR region.[13] This indicates that the color can be tuned in Cr^{3+}-doped materials by varying the host matrix.

Furthermore, as a host matrix, different oxide hosts have been explored for their utility in lighting and display devices. The zincate-based host matrix possesses good chemical and thermal stability. In this article, the calcium aluminozincate phosphor has been chosen as a host matrix since it possesses excellent luminescent properties when doped with rare earth ions. Therefore, the authors chose the same host matrix and tried to explore the luminescent behavior of the host when doped with transition metal ions.

Furthermore, there are different synthesis techniques to design phosphor materials, including the solid-state reaction method, sol–gel, combustion, hydrothermal, and molten salt. For the synthesis of the Cr^{3+}-doped calcium aluminozincate phosphor, the sol–gel technique is followed as it is a low temperature synthesis technique that provides the facility of

Department of Applied Physics, Delhi Technological University, Shahbad Daulatpur, Bawana Road, New Delhi 110 042, India. E-mail: drsrallam@gmail.com

controlling parameters during the reaction process.[21,22] Moreover, the morphology is improved with the low temperature synthesis technique in comparison with the solid-state reaction technique. This results in better luminescent properties of the prepared phosphors.

Hence, in this article, Cr^{3+}-doped calcium aluminozincate phosphors have been developed using the sol–gel technique. The structural and luminescent properties have been examined thoroughly to understand the potential of a rare earth-free phosphor in lighting applications.

2. Experiment and characterizations

$Ca_{3-x}Al_4ZnO_{10}:xCr^{3+}$ (where x = 0.01, 0.02, 0.03, 0.04 & 0.05 mol) phosphors were synthesized *via* sol–gel method. The precursors, including calcium nitrate ($Ca(NO_3)_2\cdot 9H_2O$, 99.9%), zinc nitrate ($Zn(NO_3)_2\cdot 6H_2O$, 99.9%), aluminium nitrate ($Al(NO_3)_3\cdot 6H_2O$, 99.9%) chromium(III) nitrate nonahydrate ($Cr(NO_3)_3\cdot 9H_2O$, 99.9%), and citric acid anhydrous ($C_6H_8O_7\cdot 2H_2O$, 99.5%) were dissolved individually in the de-ionized (DI) water without further purification. At first instance, the nitrates of calcium, zinc and aluminium were added by stirring at 80 °C. Then, a dropwise solution of chromium nitrate in DI water was added, and the solution was allowed to mix by placing it on a magnetic stirrer at 120 °C for 2 h. The solution of citric acid (CA) in DI was added into the above mixture. The ratio of metal nitrates to citric acid was fixed as 1 : 2, and pH = 2 was kept for this reaction to take place successfully to prepare the said phosphor. A volume of 2 ml of polyethylene glycol (PEG) was added dropwise, and the solution was stirred for 10 hours. Brown porous solid flakes were obtained after firing at 500 °C. It was ground and sintered at 1000 °C, and then again ground to carry out further characterizations.

The X-ray Bruker D8 Advance Diffractometer was used to record the XRD patterns of the synthesized phosphor, and it has the Cu source to produce the X-ray (λ = 1.54 Å). A Jasco FP-8300 spectrofluorometer was used to measure the photoluminescence emission and excitation. An Edinburgh FL920 Fluorescence Lifetime Spectrometer was used to record the photoluminescence decay profile. The FT-IR spectrum was recorded by a FT-IR Spectrometer – PerkinElmer Frontier. The temperature-dependent photoluminescence characteristics were investigated by the FLAME-S-XR1-ES model ocean optics spectrometer.

3. Results and discussion

3.1. Phase analysis

As shown in Fig. 1, X-ray diffraction (XRD) patterns of the Cr^{3+}-doped CAZ phosphor at various Cr^{3+} concentrations (0.01, 0.02, 0.03, 0.04, and 0.05 mol) are in accordance with the $Ca_3Al_4ZnO_{10}$ standard card (ICDD card no. 04-009-7304), and the (h k l) planes have been properly indexed. The synthesis of the calcium aluminozincate phosphor is confirmed by the sharp XRD patterns that are free of any extra impurity peaks. This confirms that the prepared phase is pure, and its structure matches with the orthorhombic structure.

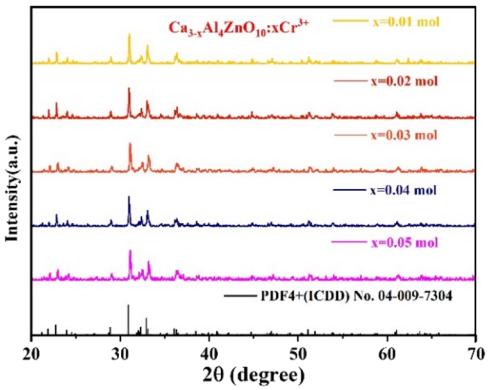

Fig. 1 XRD patterns of the synthesized CAZ samples.

According to the findings, adding Cr^{3+} ions to the calcium aluminozincate phosphor does not significantly alter the host crystal structure.

The average crystallite size of $Ca_{2.97}Al_4ZnO_{10}:0.03Cr^{3+}$ was measured by substituting the related parameters from the recorded XRD data in the Debye–Scherer equation, as reported in the literature.[23] The average crystallite size is estimated as 38 nm.

3.2. Morphology

The morphological image of $Ca_{2.97}Al_4ZnO_{10}:0.03Cr^{3+}$ is conferred in Fig. 2. The synthesized sample has a solid microcrystalline structure, which ascertains the random morphology of the particle along with some agglomeration. The average particle size of the synthesized phosphor is in the range of 1–5 μm, which is suitable for the application in lighting devices.[24]

3.3. FT-IR analysis

The functional group composition study of the synthesized CAZ phosphor was carried out by FT-IR. Fig. 3 represents the FT-IR

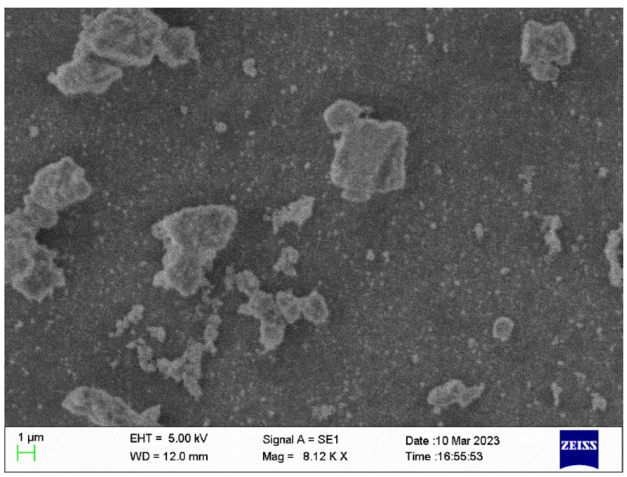

Fig. 2 SEM image of the $Ca_{2.97}Al_4ZnO_{10}:0.03Cr^{3+}$ phosphor.

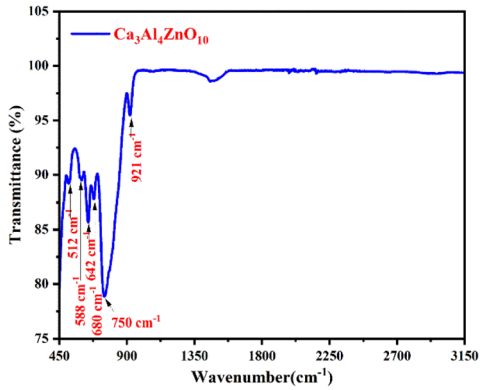

Fig. 3 FT-IR spectrum of the $Ca_{2.97}Al_4ZnO_{10}$:0.03Cr^{3+} phosphor.

spectrum of the $Ca_{2.97}Al_4ZnO_{10}$:0.03Cr^{3+} phosphor in the frequency region of 450 to 3150 cm^{-1}.

The bands in the range of 450–650 cm^{-1} appeared due to the vibration of the bond between the metal and oxygen atoms Al–O and Ca–O.[25] The characteristic bands at 512 and 588 cm^{-1} reveal the vibration of Zn–O in the stretching of the ZnO_4 unit.[26,27] The bands centered at 642, 680 cm^{-1} and 750 cm^{-1} are due to the Al–O bond vibrations in the AlO_4 tetrahedral unit.[25,28,29] The band at 921 cm^{-1} is because of the asymmetric stretch vibrations of the Al_n–OH bond.[30]

3.4. Room temperature luminescence characteristics

The photoluminescence excitation (PLE) spectrum was recorded at an emission wavelength of 688 nm, and is displayed in Fig. 4. The broad excitation peaks appear in the range of 460 to 650 nm and centered at 540 nm due to the spin-allowed transition $^4A_{2g} \rightarrow {}^4T_{2g}$.[19]

The photoluminescence (PL) spectra of the CAZ:$x$$Cr^{3+}$ phosphor were recorded by maintaining its irradiation wavelength at 540 nm for different concentrations of chromium ion, and are shown in Fig. 5. The spectra show numerous distinct peaks that are characteristic of Cr^{3+} ion emission in a strong field with

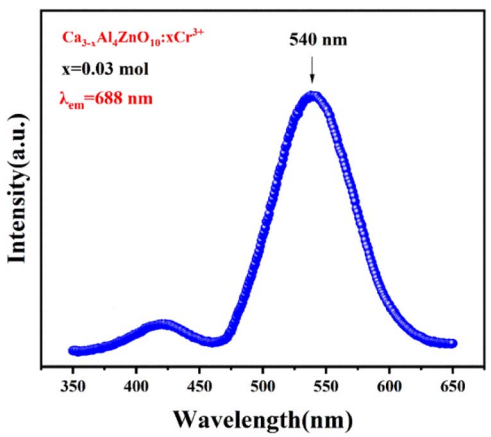

Fig. 4 PLE spectrum of the synthesized sample CAZ:$x$$Cr^{3+}$ (where x = 0.03 mol).

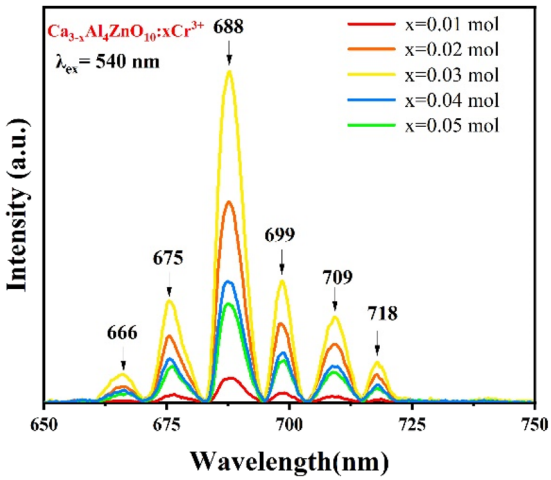

Fig. 5 PL spectra of different Cr^{3+} doping concentrations.

octahedral coordination. The sample with 0.03 mol Cr^{3+} doping shows the highest emission intensity at 688 nm. This is due to the $^2E \rightarrow {}^4A_2$ transition (zero-phonon R-line of Cr^{3+} ions).[19,31] A similar band was observed in $ZnAl_2O_4$ doped with Cr^{3+} ions, as reported by Qiang M. *et al.*[19] However, it is not the case with all of the hosts that they exhibit emission at similar wavelengths. Liu *et al.* reported on $MgTa_2O_6$:Cr^{3+} and observed a broad emission with a peak at 834 nm.[20] This occurs because the valence electrons of the transition metal ions are not shielded with the outer shell. This results in a strong interaction between the ligand field and d electrons of the transition metal ions. Thus, by altering the host, the emission can be tuned in luminescent materials that are being doped with transition metal ions. The additional emission peaks in the present study are positioned at 666 nm, 675 nm, 699 nm, 709 nm, and 718 nm, and include the R-line and the phonon sidebands.[19,31,32]

The side bands are observed due to anti-site defects, which basically arise due to thermal corrosion and anti-stoke displacement.[20] In another reported article by Xiao *et al.*, it has been shown that Cr^{3+} ions occupied multiple sites. Owing to this, there are bands observed at different positions.[17] Thus, it can be anticipated from previously published reports and the work conducted in the present study that the host matrix plays a major role in tuning the emission in Cr^{3+}-doped materials. It is thus possible to tune the emission from red to far infrared (*i.e.*, 650–1400 nm). Moreover, the luminescence intensity increases up to 0.03 mol Cr^{3+} ion doping. After that, it starts to decrease with an increase in doping concentration. This occurs due to concentration quenching. Lai *et al.* reported on a Cr^{3+}-doped $SrGa_4O_7$ host, where the emission was observed at 696 and 770 nm.[18] In general, three interaction processes, exchange interaction, radiation reabsorption, and electric multipolar interaction among activator ions are responsible for non-radiative energy transfer.[33] The exchange interaction can take place at critical distances of up to 5 Å (R_C), which is insufficient for concentration quenching at very low concentration. This cannot be ascribed to concentration quenching because there will be sufficient distance between the two luminous centers.

An event of radiation reabsorption takes place only when the excitation and emission spectra are overlapped, which is not seen in the presently studied phosphor. The electric multipole–multipole interaction is majorly affected by the critical distance. The good estimation of non-radiative transfer of energy between the Cr^{3+} ions is provided by the critical distance among Cr^{3+} and Cr^{3+} ions at the critical concentration (X_C). R_C is calculated by the equation, which is mentioned in the literature.[34,35] By using the experimental data, the critical distance is calculated to be 24 Å. The calculated R_C is much greater than 5 Å, which is required for the exchange interaction. As the critical distance is considerably different, it is obvious that the exchange interaction is an unsuitable method for transferring energy in this situation. Instead, multipolar interaction might have taken place in this host.

If the energy transfer takes place by electric multipole interaction, then it can be investigated by Dexter's theory. From Dexter's theory, the emission intensity is given by the following equation:[36]

$$\frac{I}{x} = K\left[(1+\beta(x))^{\frac{Q}{3}}\right]^{-1} \quad (1)$$

where, I is an intensity of the photoluminescence, x is a dopant ion concentration, and K and β are constants for the host lattice. The closest ion interaction type is identified by the Q value, which is equal to 3, 6, 8, and 10 for exchange, dipole–dipole, dipole-quadrupole, and quadrupole–quadrupole interactions, respectively. Simplifying the above equation by taking the log, the simplified equation is given below:

$$\log\frac{I}{x} = P - \frac{Q\log(x)}{3};\ \text{where}(P = \log K - \log\beta) \quad (2)$$

In the above equation, P is not affected by the doping concentration. The value of Q is calculated by plotting the graph between $\log(x)$ and $\log(I/x)$, which is demonstrated in Fig. 6. The as-obtained value of Q from the slope of the graph is 5.52, which is close to 6, specifying that the energy transfer occurred on account of the dipole–dipole interaction.

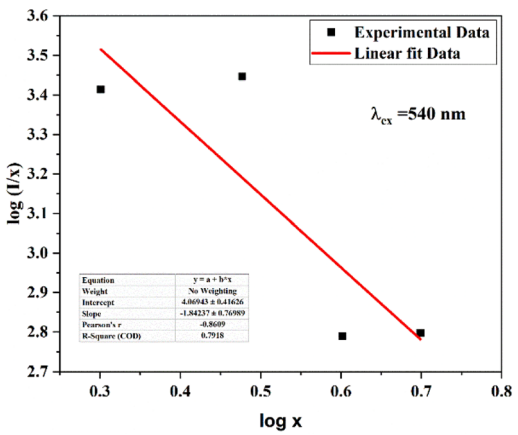

Fig. 6 Plot of $\log(I/x)$ *vs.* $\log(x)$.

The CIE 1931 diagram is a widely used system for obtaining all possible colors by using three primary colors. The CIE coordinate of all synthesized samples is calculated by using the photoluminescence data. The CIE coordinate of the synthesized CAZ:$x$$Cr^{3+}$ is shown in Table 1, and the CIE plot of the chromium-doped CAZ phosphor is shown in Fig. 7. The CIE coordinates fall in the pure red region close to the perimeter of the CIE graph, indicating the deep red emission exhibited by the prepared phosphor. These studies recommend the prospective of utilizing a chromium-doped phosphor in lighting and display devices as a red emitter.

3.5. External quantum yield

The quantum yield (QY) of a luminous material characterizes a radiative transition when combined with the luminescence lifespan, luminescence spectrum, and photostability of the phosphor. The ratio of photons released to photons absorbed by the irradiated sample is known as QY. High quantum yield phosphors are more effective in transforming the absorbed energy into emitted light, which results in brighter and more vibrant colors. For applications where efficiency is crucial, such as in lighting or solar cells, a greater quantum yield also implies that less energy is wasted as heat. The external quantum yield (EQY) of a phosphor, which demonstrates how effectively electrical power is converted to the observed optical power, is a crucial consideration. The EQY of the synthesized phosphor samples were evaluated by using eqn (3), which is given as:

$$\eta = \frac{\int \lambda P(\lambda)\mathrm{d}\lambda}{\int \lambda E(\lambda)\mathrm{d}\lambda} \quad (3)$$

where $E(\lambda)$ and $P(\lambda)$ stand for the excitation and emission spectra's intensity per wavelength, respectively.[37,38] Table 1 lists the quantum yield of the synthesized phosphor material. The efficiency of the synthesized material was shown to rise with an increase in doping up to 0.03 mol, after which it continues to decrease as the luminescence deteriorates at higher concentration due to the quenching mechanism. The EQY (η) of the $Ca_{3-x}Al_4ZnO_{10}$:$x$$Cr^{3+}$ (where x = 0.03 mol) phosphor is calculated as 46.80% under the excitation of 540 nm, which is significantly higher in comparison to previously published studies, such as the $KSrVO_4$ (EQY: 41.64%),[38] Ba_2SrWO_6:Mn^{4+} (EQY: 39.55),[39] $Mg_3Ga_2GeO_8$:Ni^{2+} (EQY: 7.3%)[40] phosphor. This relatively higher quantum yield value signifies the practical application of the phosphor under study.

Table 1 The color coordinates of CIE 1931 diagram and quantum yield

Cr^{3+} doping concentration (mol)	Color coordinates		Quantum yield (η)
	x	y	
0.01	0.7343	0.2556	35.13%
0.02	0.7334	0.2665	38.91%
0.03	0.7336	0.2662	46.80%
0.04	0.7340	0.2659	41.04%
0.05	0.7332	0.2667	32.59%

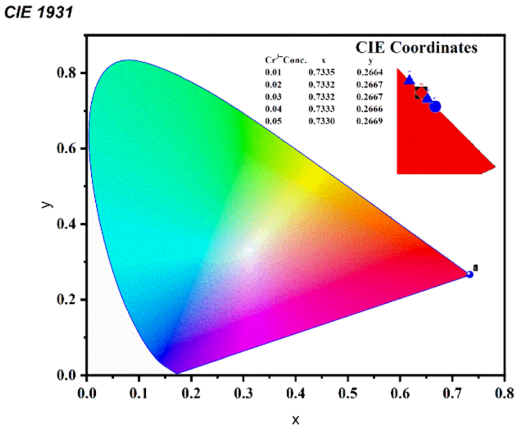

Fig. 7 CIE 1931 plot of the Cr^{3+}-doped CAZ phosphor.

3.6. Decay curve analysis

For additional evaluation of the luminescence behavior of the phosphor, fluorescence lifespan measurements were made. The fluorescence lifespan decay curve of the synthesized phosphor material with different Cr^{3+} ion concentrations is recorded by observing 688 nm emission upon 540 nm excitation. Fig. 8(a–e) manifests the decay curves of the synthesized samples, and the curves are fitted by the following tri-exponential eqn (4):

$$I_t = I_0 + B_1 \exp\left(-\frac{t}{\tau_1}\right) + B_2 \exp\left(-\frac{t}{\tau_2}\right) + B_3 \exp\left(-\frac{t}{\tau_3}\right) \quad (4)$$

For all the samples, where B_1, B_2 and B_3 are fitting parameters, I_t and I_0 are the PL intensities at time t and 0, respectively, and τ_1, τ_2 and τ_3 are the lifetimes corresponding to the fast and followed by two slow decays. The average life τ is calculated by the given formula:[28]

$$\tau = \frac{A_1\tau_1^2 + A_2\tau_2^2 + A_3\tau_3^2}{A_1\tau_1 + A_2\tau_2 + A_3\tau_3} \quad (5)$$

The average lifetime of the synthesized phosphor is calculated to be 12.08, 9.86, 3.06, 2.40, and 0.67 microseconds for 0.01, 0.02, 0.03, 0.04 and 0.05 mol Cr^{3+} ion concentration, respectively. It is observed here that the life time has decreased with the increase in Cr^{3+} ion doping concentration because of the energy transfer among the Cr^{3+} ion at shorter distances. Lifetime with Cr^{3+} ion concentration variation can be seen in Fig. 8(f).

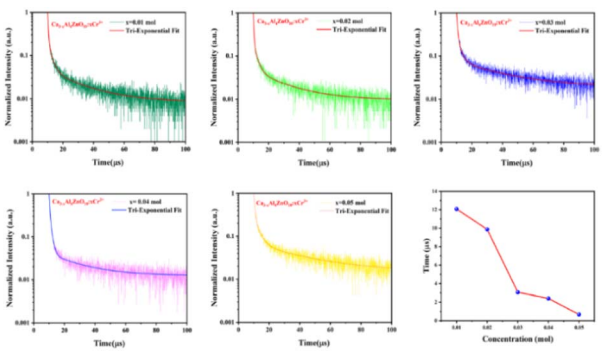

Fig. 8 Decay curves of CAZ:xCr^{3+} for different amount of Cr^{3+} ions in the host and graph of average lifetime *versus* concentration of chromium ions.

3.7. Temperature dependent photoluminescence (TD-PL)

Temperature-dependent PL spectra for the optimized $Ca_{2.97}Al_4ZnO_{10}$:$0.03Cr^{3+}$ phosphor were studied to see the impact of temperature change on the emission profile, and to gain a better understanding of the thermal stability of the aforementioned phosphor. The TD-PL spectra were measured under 540 nm excitation wavelength by alleviating the temperature from 300 to 450 K, as shown in Fig. 9. The emission intensity tends to decrease with a rise in temperature without any change in the emission spectral profile. It was observed from Fig. 9 that the PL intensity dropped by 27.4% at 450 K compared to the intensity at room temperature. The sample also shows a significant emission of 77.31% at 390 K, which is the ambient operating temperature for any practical application. Further analysis of the TD-PL of the $Ca_{2.97}Al_4ZnO_{10}$:$0.03Cr^{3+}$ phosphors to confirm the thermal stability, activation energy (ΔE) was calculated using the Arrhenius eqn (6).

$$I_T = \frac{I_0}{1 + D\exp\left(-\frac{\Delta E}{K_B T}\right)} \quad (6)$$

In this equation, I_0 stands for the emission intensity at room temperature, I_T for the emission intensity at elevated temperature (T), ΔE specifies the activation energy, K_B is the known constant given by Boltzmann, and D is an arbitrary constant. As shown in Fig. 10, the graph between $\ln((I_0/I_T) - 1)$ and $1/K_BT$ is a linear fit to estimate the activation energy (ΔE) value. The activation energy for the $Ca_{2.97}Al_4ZnO_{10}$:$0.03Cr^{3+}$ phosphor was calculated to be 0.309 eV, which is the negative of the slope as obtained from the graph.

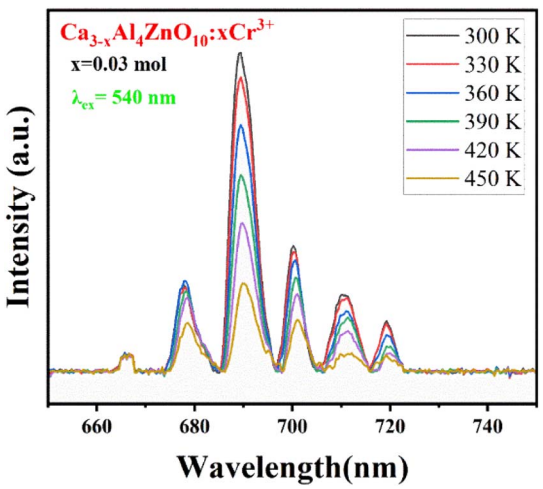

Fig. 9 Temperature-dependent emission spectra (λ_{ex} = 540 nm) of the $Ca_{2.97}Al_4ZnO_{10}$:$0.03Cr^{3+}$ phosphor at the temperature range of 300 K to 450 K.

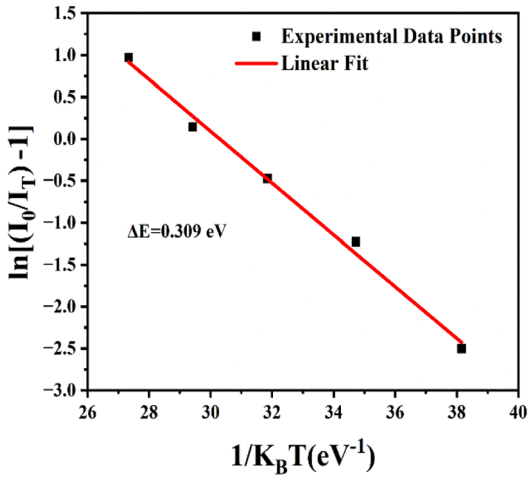

Fig. 10 Computation of the activation energy from the linear fitted plot of $\ln\left[\left(\frac{I_0}{I_T}\right)-1\right]$ and $\frac{1}{K_B T}$.

The activation energy calculated here has a higher value relative to other reported values for Ca_3WO_6:Dy^{3+} (0.105 eV), $CaAl_4O_7$:Mn^{4+} (0.196 eV), $Ca_{1.65}Sr_{0.35}SiO_4$:Ce^{3+} (0.135 eV), $Ca_3Bi(PO_4)_3$:Dy^{3+}(0.223 eV), Na_2CaSiO_4:Sm^{3+} (0.283 eV) and $Ca_9Mg_{1.5}(PO_4)_7$:Eu^{2+} (0.297 eV).[41–45] With a higher activation energy value, it can be concluded that the material has good thermal stability. Since the CAZ phosphor has good thermal stability with a relatively high value of activation energy, it shows potential for lighting and display applications.[44,46]

4. Conclusions

Cr^{3+}-doped calcium aluminozincate phosphors were efficaciously developed by sol–gel technique to study the luminescent behavior of the phosphor. The XRD patterns reveal that the phosphor has been developed in the pure phase with an orthorhombic structure, along with a random morphology of particles, as shown from the SEM image. The prepared phosphors emulate deep red emission by fixing the irradiation wavelength at 540 nm. The optimized amount of chromium ions was observed as 0.03 mol. The CIE coordinates ascertain the red emission exhibited by the prepared phosphors. The recorded decay curves and lifetime evaluation confirm that the energy transfer between the chromium ions occurs as a consequence of dipole–dipole interaction. The luminescent spectra based on temperature variation show that phosphor is thermally stable with a relatively high value of activation energy 0.309 eV. The quantum yield is 46.80% for the optimized sample. The entire study conducted on the prepared Cr^{3+}-doped CAZ phosphor indicates that it is quite appropriate for lighting and display applications.

Author contributions

Sumandeep Kaur: synthesis, data analysis and manuscript writing, Videsh Kumar: data analysis and manuscript writing, A.S. Rao: manuscript correction and supervision.

Conflicts of interest

There are no conflicts to declare.

Acknowledgements

Dr Sumandeep Kaur is grateful to the Council of Scientific and Industrial Research, New Delhi, India for providing financial support in terms of the Research Associate Fellowship (File No. 08/133(0053)/2020-EMR-I).

Notes and references

1 S. Wang, J. Zhu, Y. He, *et al.*, Invisible NIR Spectral Imaging and Laser-Induced Thermal Imaging of Na(Nd/Y)F4@glass with Opposite Effect for Optical Security, *Laser Photonics Rev.*, 2022, **16**(8), 2200039–2200046, DOI: 10.1002/lpor.202200039.

2 E. Rai, R. S. Yadav, D. Kumar, A. K. Singh, V. J. Fulari and S. B. Rai, Effect of Cr^{3+} doping on structural and optical properties of Eu^{3+} doped $LaVO_4$ phosphor, *RSC Adv.*, 2023, **13**(7), 4182–4194, DOI: 10.1039/d2ra06962h.

3 C. Kumari, A. Kumar, S. K. Sharma and J. Manam, Sr_3LiSbO_6:Er^{3+} phosphors for green LEDs and solar cell applications, *Vacuum*, 2023, **207**, 111599, DOI: 10.1016/j.vacuum.2022.111599.

4 W. Xia, H. Cheng, Q. Mao, *et al.*, Improving the luminescence performance of far-red-emitting Sr_2ScSbO_6:Mn^{4+} phosphor with charge compensation and its application in plant growth LEDs, *Ceram. Int.*, 2023, **49**(9PA), 13708–13716, DOI: 10.1016/j.ceramint.2022.12.249.

5 D. Liu, Effects of Cr content and morphology on the luminescence properties of the Cr-doped alpha-Al_2O_3 powders, *Ceram. Int.*, 2013, **39**(5), 4765–4769, DOI: 10.1016/j.ceramint.2012.11.063.

6 Y. R. S. Monika, A. Bahadur and S. B. Rai, Concentration and pump power-mediated color tunability, optical heating and temperature sensing via TCLs of red emission in an Er^{3+}/Yb^{3+}/Li^+ co-doped $ZnGa_2O_4$ phosphor, *RSC Adv.*, 2019, **9**(68), 40092–40108, DOI: 10.1039/c9ra09120c.

7 H. Huang, R. Li, S. Jin, *et al.*, Ytterbium-Doped $CsPbCl_3$ Quantum Cutters for Near-Infrared Light-Emitting Diodes, *ACS Appl. Mater. Interfaces*, 2021, **13**(29), 34561–34571, DOI: 10.1021/acsami.1c09421.

8 J. Zhong, D. Chen, X. Chen, *et al.*, Efficient rare-earth free red-emitting Ca_2YSbO_6:Mn^{4+}, M(M = Li^+, Na^+, K^+, Mg^{2+}) phosphors for white light-emitting diodes, *Dalton Trans.*, 2018, **47**(18), 6528–6537, DOI: 10.1039/c8dt00992a.

9 S. Jin, R. Li, H. Huang, *et al.*, Compact ultrabroadband light-emitting diodes based on lanthanide-doped lead-free double perovskites, *Light: Sci. Appl.*, 2022, **11**(1), 1–21, DOI: 10.1038/s41377-022-00739-2.

10 Z. Zhou, N. Zhou, M. Xia, M. Yokoyama and H. T. Hintzen, Research progress and application prospects of transition metal Mn4+-activated luminescent materials, *J. Mater. Chem. C*, 2016, **4**(39), 9143–9161, DOI: 10.1039/c6tc02496c.

11 J. Jiang, T. Xu, J. Lu, L. Sun and Z. Ni, Review Article, *Defect Engineering in 2D Materials : Precise Manipulation and Improved Functionalities*, 2019, 2019, DOI: 10.34133/2019/4641739.

12 C. S. Kamal, T. K. Visweswara Rao, T. Samuel, *et al.*, Blue to magenta tunable luminescence from LaGaO3: Bi3+, Cr3+ doped phosphors for field emission display applications, *RSC Adv.*, 2017, **7**(71), 44915–44922, DOI: 10.1039/c7ra08864g.

13 G. Liu, M. S. Molokeev, B. Lei and Z. Xia, Two-site Cr3+occupation in the MgTa2O6:Cr3+phosphor toward broad-band near-infrared emission for vessel visualization, *J. Mater. Chem. C*, 2020, **8**(27), 9322–9328, DOI: 10.1039/d0tc01951h.

14 L. Wang, Z. Dai, R. Zhou, B. Qu and X. C. Zeng, Understanding the quenching nature of Mn^{4+} in wide band gap inorganic compounds: design principles for Mn^{4+} phosphors with higher efficiency, *Phys. Chem. Chem. Phys.*, 2018, **20**(25), 16992–16999, DOI: 10.1039/c8cp02569j.

15 J. Orive, R. Balda, J. Fernández, L. Lezama and M. I. Arriortua, Low temperature red luminescence of a fluorinated Mn-doped zinc selenite, *Dalton Trans.*, 2013, **42**(34), 12481–12494, DOI: 10.1039/c3dt51224j.

16 R. Boonsin, G. Chadeyron, J. P. Roblin, D. Boyer and R. Mahiou, Development of rare-earth-free phosphors for eco-energy lighting based LEDs, *J. Mater. Chem. C*, 2015, **3**(37), 9580–9587, DOI: 10.1039/c5tc01516b.

17 F. Xiao, C. Xie, S. Xie, R. Yi, H. Yuan and H. Zhou, Multi-site Cr3+occupation-related broadband NIR luminescence in Cr^{3+}-doped $Li_3Mg_2NbO_6$, *CrystEngComm*, 2021, **23**(33), 5585–5594, DOI: 10.1039/d1ce00746g.

18 J. Lai, J. Qiu, Q. Wang, *et al.*, Disentangling site occupancy, cation regulation, and oxidation state regulation of the broadband near infrared emission in a chromium-doped $SrGa_4O_7$ phosphor, *Inorg. Chem. Front.*, 2020, **7**(12), 2313–2321, DOI: 10.1039/d0qi00332h.

19 M. Qiang, X. Yin, H. Lin, *et al.*, $ZnAl_2O_4:Cr^{3+}$ translucent ceramic phosphor with thermally stable far-red luminescence, *Opt. Mater.*, 2022, **133**, 112887, DOI: 10.1016/j.optmat.2022.112887.

20 J. Zhong, L. Zeng, W. Zhao and J. Brgoch, Producing Tunable Broadband Near-Infrared Emission through Co-Substitution in $(Ga_{1-x}Mg_x)(Ga_{1-x}Ge_x)O_3:Cr^{3+}$, *ACS Appl. Mater. Interfaces*, 2022, 10–17, DOI: 10.1021/acsami.2c17902.

21 M. I. Miranda-López, F. F. Contreras-Torres, D. Cavazos-Cavazos, *et al.*, Crystal evolution of nano-sized $CoCr_2O_4$ synthesized by a modified sol–gel method, *J. Phys. Chem. Solids*, 2023, **178**, 111315, DOI: 10.1016/j.jpcs.2023.111315.

22 P. M. Kakade, A. R. Kachere, P. D. Sahare, *et al.*, Structural, compositional and luminescence studies of Y2O3:Eu3+ nanophosphor synthesized by sol-gel method, *J. Alloys Compd.*, 2022, **928**, 167106, DOI: 10.1016/j.jallcom.2022.167106.

23 S. Kaur, A. S. Rao, M. Jayasimhadri, B. Sivaiah and D. Haranath, Synthesis optimization, photoluminescence and thermoluminescence studies of Eu3+ doped calcium aluminozincate phosphor, *J. Alloys Compd.*, 2019, **802**, 129–138, DOI: 10.1016/j.jallcom.2019.06.169.

24 Y. Li, Z. Zhao, Z. Song, R. Wan, J. QIu, Z. Yang, Z. Yin, X. Liu, Q. Liu and Y. Zhou, Far-Red-Emitting BiOCl Eu3 Phosphor with Excellent Broadband.pdf, *J. Am. Ceram. Soc.*, 2015, **98**(7), 2170–2176, DOI: 10.1111/jace.13589.

25 J. Suresh Kumar, K. Pavani, A. Mohan Babu, N. Kumar Giri, S. B. Rai and L. R. Moorthy, Fluorescence characteristics of Dy^{3+} ions in calcium fluoroborate glasses, *J. Lumin.*, 2010, **130**(10), 1916–1923, DOI: 10.1016/j.jlumin.2010.05.006.

26 G. P. Singh, S. Kaur, P. Kaur and D. P. Singh, Modification in structural and optical properties of ZnO, CeO_2 doped $Al_2O_3PbOB_2O_3$ glasses, *Phys. B*, 2012, **407**(8), 1250–1255, DOI: 10.1016/j.physb.2012.01.114.

27 R. P. S. Chakradhar, B. M. Nagabhushana, G. T. Chandrappa, K. P. Ramesh and J. L. Rao, Solution combustion derived nanocrystalline Zn2SiO 4:Mn phosphors: A spectroscopic view, *J. Chem. Phys.*, 2004, **121**(20), 10250–10259, DOI: 10.1063/1.1808420.

28 S. Kaur, A. S. Rao and M. Jayasimhadri, Spectroscopic and photoluminescence characteristics of Sm3+ doped calcium aluminozincate phosphor for applications in w-LED, *Ceram. Int.*, 2017, **43**(10), 7401–7407, DOI: 10.1016/j.ceramint.2017.02.129.

29 P. Colomban, Structure of oxide gels and glasses by infrared and raman scattering – Part 1 Alumina, *J. Mater. Sci.*, 1989, **24**(8), 3002–3010, DOI: 10.1007/BF02385660.

30 E. I. Firsov and P. A. Shafranovsky, IR reflection-absorption study of O2 and H2O interaction with evaporated aluminum films, *Surf. Sci.*, 1991, **244**(1–2), 3–5, DOI: 10.1016/0039-6028(91)90163-M.

31 N. T. Huyen, M. T. Tran, N. Van Quang, *et al.*, Far-red-emitting Cr^{3+}-doped $CaAl_{12}O_{19}$ phosphors with excellent color purity and good quantum efficiency for plant growth LEDs, *Opt. Mater.*, 2022, **133**, 113002, DOI: 10.1016/j.optmat.2022.113002.

32 A. Bessière, S. Jacquart, K. Priolkar, A. Lecointre, B. Viana and D. Gourier, ZnGa_2O_4:Cr^3+: a new red long-lasting phosphor with high brightness, *Opt. Express*, 2011, **19**(11), 10131, DOI: 10.1364/oe.19.010131.

33 D. L. Dexter, *A Theory of Sensitized Luminescence in Solids Articles you may be interested in A Theory of Sensitized Luminescence in Solids*, 2004, 1953, p. 836, DOI: 10.1063/1.1699044.

34 Maheshwary, B. P. Singh, J. Singh and R. A. Singh, Luminescence properties of Eu3+-activated SrWO4 nanophosphors-concentration and annealing effect, *RSC Adv.*, 2014, **4**(62), 32605–32621, DOI: 10.1039/c4ra05903d.

35 Z. Ci, Q. Sun, S. Qin, *et al.*, Warm white light generation from a single phase Dy^{3+} doped Mg2Al4Si5O18 phosphor for white UV-LEDs, *Phys. Chem. Chem. Phys.*, 2014, **16**(23), 11597–11602, DOI: 10.1039/c4cp00357h.

36 S. Kaur, M. Jayasimhadri and A. S. Rao, A novel red emitting Eu3+doped calcium aluminozincate phosphor for applications in w-LEDs, *J. Alloys Compd.*, 2017, **697**, 367–373, DOI: 10.1016/j.jallcom.2016.12.150.

37 W. Li, R. J. Xie, T. Zhou, L. Liu and Y. Zhu, Synthesis of the phase pure $Ba_3Si_6O_{12}N_2$:Eu^{2+} green phosphor and its application in high color rendition white LEDs, *Dalton Trans.*, 2014, **43**(16), 6132–6138, DOI: **10.1039/c3dt53603c**.

38 P. Sharma, P. Singh and Kamni, Study of synthesis mechanism, structural, optical and luminescent properties of bluish-violet rare earth doped KSrVO4: Nd3+ nano powders, *Mater. Sci. Eng. B: Solid-State Mater. Adv. Technol.*, 2022, **276**, 115564, DOI: **10.1016/j.mseb.2021.115564**.

39 Y. Zhang, C. Zhou, J. Li, *et al.*, Realization of highly efficient Ba_2SrWO_6:Mn^{4+} phosphor via La addition strategy and application for plant cultivation LED, *J. Alloys Compd.*, 2023, **937**, 168418, DOI: **10.1016/j.jallcom.2022.168418**.

40 C. Wang, J. Lin, X. Zhang, *et al.*, Efficient ultra-broadband NIR-II emission achieved by multi-site occupancy in Mg_3Ga_2GeO8: Ni^{2+} phosphor, *J. Alloys Compd.*, 2023, **942**, 168893, DOI: **10.1016/j.jallcom.2023.168893**.

41 D. Xu, Z. Yang, J. Sun, X. Gao and J. Du, Synthesis and luminescence properties of double-perovskite white emitting phosphor Ca_3WO_6:Dy^{3+}, *J. Mater. Sci.: Mater. Electron.*, 2016, **27**(8), 8370–8377, DOI: **10.1007/s10854-016-4848-z**.

42 K. Li, M. Shang, H. Lian and J. Lin, Photoluminescence Properties of Efficient Blue-Emitting Phosphor α-$Ca_{1.65}Sr_{0.35}SiO_4$:Ce^{3+}: Color Tuning via the Substitutions of Si by Al/Ga/B, *Inorg. Chem.*, 2015, **54**(16), 7992–8002, DOI: **10.1021/acs.inorgchem.5b01197**.

43 P. Li, M. Peng, X. Yin, *et al.*, Temperature dependent red luminescence from a distorted Mn^4+ site in CaAl_4O_7:Mn^4+, *Opt. Express*, 2013, **21**(16), 18943, DOI: **10.1364/oe.21.018943**.

44 H. Kaur, M. Jayasimhadri, M. K. Sahu, P. K. Rao and N. S. Reddy, Synthesis of orange emitting Sm^{3+} doped sodium calcium silicate phosphor by sol-gel method for photonic device applications, *Ceram. Int.*, 2020, **46**(16), 26434–26439, DOI: **10.1016/j.ceramint.2020.04.224**.

45 R. Mi, Y. Liu, L. Mei, *et al.*, Multi-site occupancies and dependent photoluminescence of $Ca_9Mg_{1.5}(PO_4)_7$:Eu^{2+} phosphors: A bifunctional platform for optical thermometer and plant growth lighting, *J. Rare Earths*, 2022, **5**, DOI: **10.1016/j.jre.2022.06.009**.

46 V. Singh, S. Kaur and M. Jayasimhadri, Luminescence properties of orange emitting $CaAl_4O_7$:Sm^{3+} phosphor for solid state lighting applications, *Solid State Sci.*, 2020, **101**, 106049–106054, DOI: **10.1016/j.solidstatesciences.2019.106049**.